Am J Transl Res 2021;13(5):4437-4449
www.ajtr.org /ISSN:1943-8141/AJTR0120267

Original Article

Quantitative ultrasound characterization of therapy response in prostate cancer in vivo

Deepa Sharma[1,2,3], Laurentius Oscar Osapoetra[1,2,3], Mateusz Faltyn[1], Natalie Ngoc Anh Do[1], Anoja Giles[1], Martin Stanisz[1], Lakshmanan Sannachi[1,2,3], Gregory J Czarnota[1,2,3]

[1]Imaging Research and Physical Sciences, Sunnybrook Health Sciences Centre, Toronto, Ontario, Canada; [2]Department of Radiation Oncology, Sunnybrook Health Sciences Centre, Toronto, Ontario, Canada; [3]Department of Medical Biophysics and Radiation Oncology, University of Toronto, Toronto, Ontario, Canada

Received August 13, 2020; Accepted February 17, 2021; Epub May 15, 2021; Published May 30, 2021

Abstract: Quantitative ultrasound (QUS) is a non-invasive imaging modality that permits the detection of tumor response following various cancer therapies. Based on ultrasound signal scattering from the biological system, scatterer size, and concentration of microscopic scatterers, QUS enables the rapid characterization of tumor cell death. In this study, tumor response to ultrasound-stimulated microbubbles (USMB) and hyperthermia (HT) in tumor-bearing mice, with prostate cancer xenografts (PC3), was examined using QUS. Treatment conditions included 1% (v/v) Definity microbubbles stimulated at ultrasound pressures (0, 246, and 570 kPa) and HT treatment (0, 10, 40, and 50 minutes). Three ultrasound backscatter parameters, mid-band fit (MBF), 0-MHz spectral intercept (SI), and spectral slope (SS) were estimated prior to, and 24 hours after treatment. Additionally, histological assessment of tumor cell death and tissue microstructural changes was used to complement the results obtained from ultrasound data. Results demonstrated a significant increase in QUS parameters (MBF and SI) followed combined USMB and HT treatment ($P<0.05$). In contrast, the backscatter parameters from the control (untreated) group, and USMB only group showed minimal changes ($P>0.05$). Furthermore, histological data demonstrated increased cell death and prominent changes in cellular and tissue structure, nucleus size, and subcellular constituent orientation followed combined treatments. The findings suggested that QUS parameters derived from the ultrasound backscattered power spectrum may be used to detect HT treatment effects in prostate cancer tumors *in vivo*.

Keywords: Cell death, hyperthermia, quantitative ultrasound, and ultrasound-stimulated microbubbles

Introduction

Different forms of cell death including apoptosis, autophagy, necrosis, oncosis, mitosis-linked cell death, and coagulative necrosis have been recognized [1-3]. These different forms of cell death can be easily misclassified as they share similar morphological and biochemical features. However, each form of cell death is known to have unique cellular responses to cell death that change their ultrasound scattering properties that can be detected using ultrasound [4, 5]. And hence, determining these unique changes during the cell death process is critical in monitoring treatment efficacy and developing a treatment plan [6-8].

Several *in vitro*, *in situ*, and *in vivo* studies have now confirmed that quantitative ultrasound (QUS) can be used to identify and quantify cell death using conventional (5-10 MHz) or high-frequency ultrasound (>10 MHz) [5, 9-12]. QUS is a non-invasive, inexpensive, and portable imaging modality that is frequently used for research as well as in the clinic for cancer imaging [13]. Over the past decade, QUS has been used extensively in preclinical studies to discriminate between different forms of cell death and characterizing tumor responses in terms of apoptotic cells versus viable cells [4, 11]. It has been demonstrated earlier that the frequency-dependent data contained in the radiofrequency (RF) signal can be related to the morphological changes in tissues and their microstructure. Several QUS spectral parameters specifically mid-band fit (MBF), 0-MHz spectral intercept (SI), and spectral slope (SS) can be easily determined by spectral analysis of ultrasound data.

These spectral parameters change with cell death related to decreases in scatterer size, increases in scatterer number, and changes in scatterer backscatter co-efficient resulting in overall increases in ultrasound backscatter with cell-death-inducing treatments. Specifically, these changes in QUS spectral parameters have been linked to the condensation of deoxyribonucleic acid (DNA) leading to pyknosis and karyorrhexis ultimately resulting in apoptotic cell death primarily reported following chemotherapy treatment. Previous studies have demonstrated significant increment in backscatter intensity for cells undergoing apoptosis compared to viable cells [5, 9]. Similarly, such observations with an increase in ultrasound backscatter intensity were also reported as a result of a mitotic arrest or oncosis [14-16, 28].

Clinical translational applicability of QUS

Diagnostic delay in cancer might contribute to its progression, metastasis, and poor long-term survival. Currently, patient responses to cancer treatment are clinically assessed by physical examination or using techniques that might take several weeks or months and remain an expensive approach. In contrast, functional imaging techniques can be applied to access tumor microstructure heterogeneity, tumor physiology, and determine treatment response within a short span of time. Studies suggest that QUS spectroscopic methods can easily be implemented for the characterization of tumor response non-invasively [17-20]. A study by Sadeghi-Naini *et al.* incorporated QUS to study the response to neoadjuvant chemotherapy (NAC) in locally advanced breast cancer (LABC) patients. Two ultrasound backscatter parameters MBF and SI were estimated from tumors prior to treatment (week 0/baseline) and at weeks 1, 4, and 8 during the chemotherapy session. Results demonstrated that both parameters increased significantly in patients that responded to treatment compared to nonresponding patients. An increase in MBF was 3.5 ± 1.1 dBr in the first week, 9.1 ± 1.2 dBr in the fourth week, and 8.6 ± 1.4 dBr in the eighth week compared to 1.2 ± 2.3 dBr observed preoperatively. Similarly, an increase in SI with ($P<0.05$) was reported in patients that responded to treatment. Furthermore, the backscatter changes observed in responding patients strongly correlated with the histological findings, demonstrating significant apoptotic cell death obtained from tumor specimens [17]. Evidence from other studies suggests that QUS techniques can be used to distinguish between normal versus tumor tissue as well as to characterize benign versus malignant breast lesions [19-23]. QUS texture-analysis techniques have been applied to quantify the spatial heterogeneities within a tumor allowing rapid assessment between malignant lesions that depicts heterogeneous internal echotexture compared to benign lesions with homogeneous internal echoes. Thus, this ultrasound-based functional imaging method helps in tracking cancer progression and evaluating treatment response which may allow switching of an ineffective treatment to a more effective one if required as early as possible.

The present study aims to build on previous findings that demonstrated an increase in ultrasound backscatter intensity and changes in spectral parameters that were found to be linked to tissue structural changes at cellular level following treatments using ultrasound-stimulated microbubbles (USMB) and radiation [24, 25]. The hypothesis tested in the study here is that a similar synergy between treatments should be present when hyperthermia (HT) is used in combination with USMB. Specifically, the work here investigated the treatment effect of USMB combined with HT to assess cell death in prostate cancer xenografts. As imaging surrogates of response, backscatter parameters (MBF, SI, and SS) were derived from ultrasound RF data and correlated with histological findings. Furthermore, the effect of different treatment parameters including ultrasound pressures and HT durations was also investigated in this study.

Materials and methods

Cell culture

A Prostate cancer cell line (PC3) obtained from American Type Culture Collection (ATCC, Manassas VA, USA) was cultured in RPMI-1640 (Wisent Inc., St. Bruno, Canada) media supplemented with 10% fetal bovine serum (Sigma-Aldrich, St. Louis, MO, USA) and 5% penicillin/streptomycin antibiotic (Sigma-Aldrich). Cells were cultured and maintained at 37°C and 5% (v/v) CO_2 to be allowed to reach confluence.

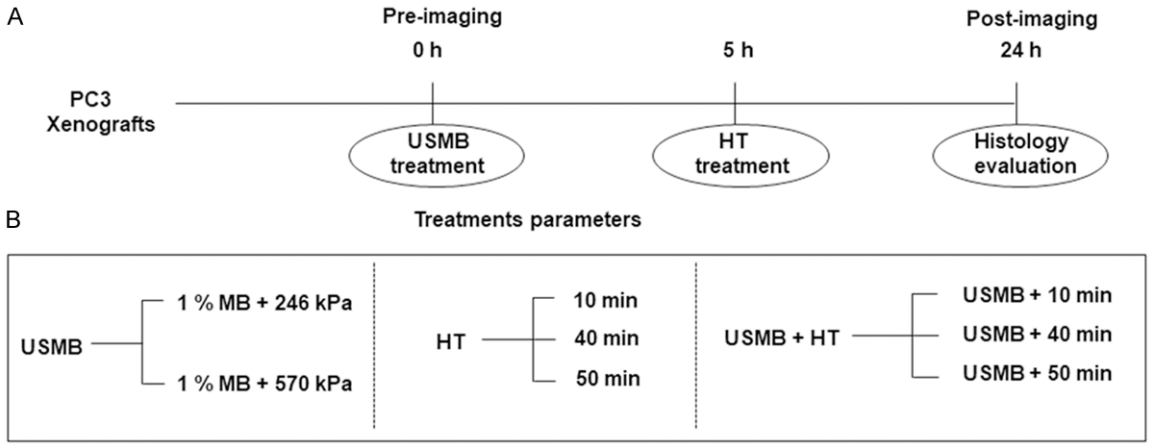

Figure 1. Schematic representation of experimental design. (A) Overview of different treatments (USMB and HT) timings and imaging time points (pre- and post-24 hours). (B) Different experimental treatment conditions (USMB only, HT only, and USMB + HT). h = hour; HT = hyperthermia; min = minutes; USMB = ultrasound-stimulated microbubbles.

Cells were subsequently harvested using 0.02% (w/v) ethylenediaminetetraacetic acid (EDTA) and 0.25% trypsin (v/v) solutions at room temperature. In preparation for injection, cells were isolated and centrifuged at 200 g, 4°C for 10 minutes (min) and resuspended in 100 µl phosphate-buffered saline (PBS) to a concentration of 5×10^6.

Animal model

All animal research was conducted in compliance with guidelines set by the Canadian Council on Animal Care and Sunnybrook Research Institute Institutional Animal Care and Use Committee. Five to six-week old CB-17 severe combined immunodeficiency (SCID) male mice (Charles River Inc., Wilmington, MA, USA) were used in this study. Animals were injected with a total cell volume of 5×10^6 cells subcutaneously into the lower right hind leg. Tumors were allowed to develop for approximately 3-4 weeks before reaching an average diameter of 8-10 mm for experiments.

Prior to treatment, animals were anesthetized using a combination of 2% (v/v) oxygen ventilated isoflurane and intraperitoneal injection with a mixture of ketamine (100 mg/kg body weight), xylazine (5 mg/kg body weight), and acepromazine (1 mg/kg body weight) (Sigma, Burlington, ON, Canada). In order to maintain optimal body temperature and to keep animals warm, heating pads and lamps were used. Mice were closely monitored, and oxygen was administered to any animals appearing to have irregular breathing.

Ethics statement

All experiments were conducted in accordance with the policies of the animal care committee at Sunnybrook Health Science Centre (Comparative Research), under animal use protocol #18-395. Throughout the experimental procedure, animals were visually monitored and handled with proper care to minimize potential suffering or pain. All the animals used in scientific research were euthanized at the end of the study by anesthetic overdose followed by cervical dislocation, as standard operating procedures.

Experimental design

Tumor response to USMB and HT treatments was assessed 24 hours after treatment. Treatments included: USMB only, HT only (10, 40, and 50 min), and a combination of USMB and HT. 0 kPa + 0 min was considered as control (untreated group). For each treatment condition, 3-5 animals were used in this study. Overview of different treatment parameters and treatment timings are illustrated in **Figure 1**.

Ultrasound and microbubble treatment

For this study, 1% (v/v) Definity® microbubbles (perfluoropropane gas/liposome shell, Lantheus Medical Imaging, Inc., North Billerica, MA,

USA) were used which were stimulated at 246 kPa or 570 kPa ultrasound pressure. Animals to be treated with microbubbles and microbubble/hyperthermia combination treatments were fitted with a tail vein catheter to permit the injection of microbubbles and saline. After the initial microbubble injection, mice received a second injection of 150 µl 0.2% heparin/saline to flush the tail vein catheter. Prior to injection microbubbles were activated using a Vialmix (Lantheus Medical Imaging, North Billerica, MA, USA) device operated at 3000 rpm for 45 seconds.

The ultrasound therapy system consisted of a digital acquisition system (Acquiris CC103, Agiulent Technologies NY), a waveform generator (AWG520, Tektronix), an amplifier (RPR-4000, Ritec Inc.), and a transducer with 28.6 mm aperture diameter operating at 500 kHz frequency. Each mouse was mounted on a custom stage with the lower body being immersed in a 37°C water bath. The tumor-bearing hind leg of each animal was exposed to ultrasound immediately after microbubble injection in such a way that a tumor was placed within the half-maximum peak of the acoustic signal. Tumors were treated for a total of 5 min, being exposed to a 16-cycle tone burst at 500 kHz with a 3 kHz pulse repetition frequency, resulting in an average duty cycle of 0.25%. Acoustic bursts were repeated every 2 seconds to allow blood vessels to refill with microbubbles between sonication, causing bubble bursting *in vivo*.

Hyperthermia treatment

For HT treatments, animals were subjected to heating at five hours following ultrasound microbubble treatments. Animals were mounted in 50 ml custom made tubes that had a hole at the bottom to act as an air vent, and a hole in the opening lid for the leg and tail to go through, and a strip of Velcro. The tail and treatment leg with the target tumor of each mouse was fixed using tape and attached to a customized plate with corresponding Velcro attachments with which to affix tubes. The plate was immersed into the water bath, held in place by a three-prong extension clamp attached to a support stand. The tumor bearing leg of each mouse was submerged into the water for their respective treatment times of 10, 40, or 50 min.

Data acquisition and analysis

Ultrasound radiofrequency (RF) data were collected 24 hours before and after the treatment using a Vevo 770 ultrasound system (Visual Sonics, Toronto, Canada). The system was equipped with an RMV-710B transducer of 25 MHz center frequency. The axial and lateral resolutions of the system were 54 µm and 149 µm, respectively. RF and B-Mode data were collected with approximately 60-100 frames acquired per scan.

Ten regions of interest (ROIs) from the ultrasound RF data were selected for QUS spectral analysis. These ROIs corresponded to 10 imaging planes within the tumor volume. The ROIs were selected for occupying approximately the majority of tumor cross-sectional area in the ultrasound images (5-10 mm × 5-10 mm in-plane and 5-10 mm through-plane regions approximately). QUS spectral parameters were obtained at each frame (10 frames per animal/tumor) and spectral data were averaged across the ultrasound scan. For each ROI, QUS spectral parametric images were created using a sliding window technique. The parametric maps reflect the spatial distribution of acoustic scatterer properties. These acoustic properties have been demonstrated to be altered as a result of cell death as the tumor responds to cancer therapies. We used a 10λ by 10λ sliding window and an 80% overlap between adjacent windows in axial and lateral directions. Here, λ is the wavelength of the transducer. A Hanning gating function was applied on individual RF scan lines within the sliding window. An averaged power spectrum was calculated from gated RF signals by taking the square magnitude of the Fast Fourier Transform (FFT). In order to remove ultrasound system-dependent effects, we performed a spectral normalization procedure using a reference phantom technique. The reference phantom consisted of glass beads with 3.3 ± 2.2 µm mean diameter ± standard deviation, immersed in agar. This tissue-equivalent phantom was scanned using the same ultrasound system and transducer and data acquisition settings.

As ultrasound attenuation from intervening tissue layers and the tumor can alter the spectral parameters, attenuation compensation was performed on the normalized power spectrum

using the assumed attenuation coefficients of 2 dB/cm/MHz and 0.6 dB/cm/MHz for the skin and the tumor, respectively. This analysis bandwidth corresponded to a frequency range of approximately 10 MHz to 25 MHz. Linear regression analysis of log-compressed, attenuation-compensated, normalized power spectrum over the frequency bandwidth 10 MHz-25 MHz resulted in QUS spectral parameters including MBF, SI, and SS.

Histopathology

Mice were euthanized and tumor specimens were excised after 24 hours for tissue staining. All excised tumor samples were sectioned into halves, with one half fixed in 10% (v/v) neutral buffered formalin (Fisher Scientific Canada, Ottawa Ontario, Canada) and the other half fixed in optical gel Tissue-Tek® O.C.T (Sakura Finetek, USA) and subsequently flash-frozen with liquid nitrogen. Formalin-fixed tumor samples were stored at room temperature for 48 hours, then were transferred into 70% ethanol (v/v) solution and stored at 4°C for 24 hours. Samples were stained using hematoxylin and eosin (H&E) for the identification of cellular and tissue structure and terminal dUTP nick-end labeling (TUNEL) to detect apoptotic cells. All the staining was performed in Pathology Research Program, University Health Network, Toronto, ON, Canada. All the images for H&E and TUNEL were captured and digitized using a Leica CD100 microscope (1 MPixel Leica DC100 video camera, 2 GHz PC operating Leica IM1000 software) and a 20 × objective lens. For TUNEL cell death quantification, digitized image files were run through an in-house program developed in MATLAB (Mathworks, Natick, MA, USA). The cell death index was quantified from digitized TUNEL image files using an in-house custom code developed in MATLAB.

Results

Changes in quantitative ultrasound parametric maps and ultrasound parameters following ultrasound-stimulated microbubbles and hyperthermia treatment

In this study tumor response to therapy was monitored using both non-invasive QUS imaging methods and immunohistochemistry. Representative parametric images for PC3 tumor xenograft following treatment are displayed in **Figure 2A**. The images show significant increases in the backscatter intensity in the combined treatment groups, particularly for 246 kPa + 40 min, 246 kPa + 50 min, 570 kPa + 40 min, and 570 kPa + 50 min treatment groups compared to the groups that were treated with control and HT only (0 kPa + 0 min, 0 kPa + 10 min, 0 kPa + 40 min, 0 kPa + 50 min). Parametric maps indicated heterogeneity of response within the tumors, as expected. Furthermore, changes associated with response in terms of changes in MBF appeared to become greater with increasing treatment time and increased with increases in ultrasound pressure. **Figure 2B** presents results indicating changes in MBF following different treatments consisting of USMB alone, HT alone, and combinations of USMB and HT. In the control group (0 kPa + 0 min), the change in MBF was -0.6 ± 0.4 dBr (mean ± standard error). For the USMB alone treatment groups, the changes in MBF were -0.8 ± 0.5 dBr and -0.3 ± 0.4 dBr for 246 kPa + 0 min and 570 kPa + 0 min, respectively. For HT treated tumor, the changes in MBF were -0.0 ± 0.3 dBr, 0.1 ± 0.4 dBr, 0.4 ± 0.5 dBr for 10, 40, and 50 min of treatment, respectively. For the combined USMB and HT treated group, the increases in MBF were 0.7 ± 0.2 dBr ($P<0.05$) for 246 kPa + 10 min; 1.4 ± 0.3 dBr ($P<0.05$) for 246 kPa + 40 min, and 1.6 ± 0.2 dBr ($P<0.05$) for 246 kPa + 50 min. Similarly, treatment with 570 kPa also demonstrated increases in MBF exhibiting values for 570 kPa + 10 min of 0.7 ± 0.2 dBr ($P<0.05$); for 570 kPa + 40 min of 1.4 ± 0.1 dBr ($P<0.05$) and for 570 kPa + 50 min a value of 1.5 ± 0.2 dBr ($P<0.05$). Changes in SI are presented in **Figure 2C**. In the control group (0 kPa + 0 min), the change in SI was -0.8 ± 0.6 dBr. For the USMB alone, the changes in SI were -0.9 ± 0.6 dBr and -0.2 ± 0.4 dBr for 246 kPa and 570 kPa groups, respectively. Similar to MBF, combined treatment of USMB and HT exhibited increases in SI intensity of 0.3 ± 0.1 dBr, 0.5 ± 0.4 dBr ($P<0.05$), and 0.7 ± 0.4 dBr ($P<0.05$) for 246 kPa + 10 min, 246 kPa + 40 min, and 246 kPa + 50 min, respectively. Alongside these, significant increases in SI of 1.0 ± 0.3 dBr ($P<0.05$), 1.2 ± 0.3 dBr ($P<0.05$) and 1.2 ± 0.8 dBr ($P<0.05$) were also observed for the 570 kPa + 10 min, 570 kPa + 40 min, and 570 kPa + 50 min, respectively. A one-way ANOVA with Bonferroni selected comparison

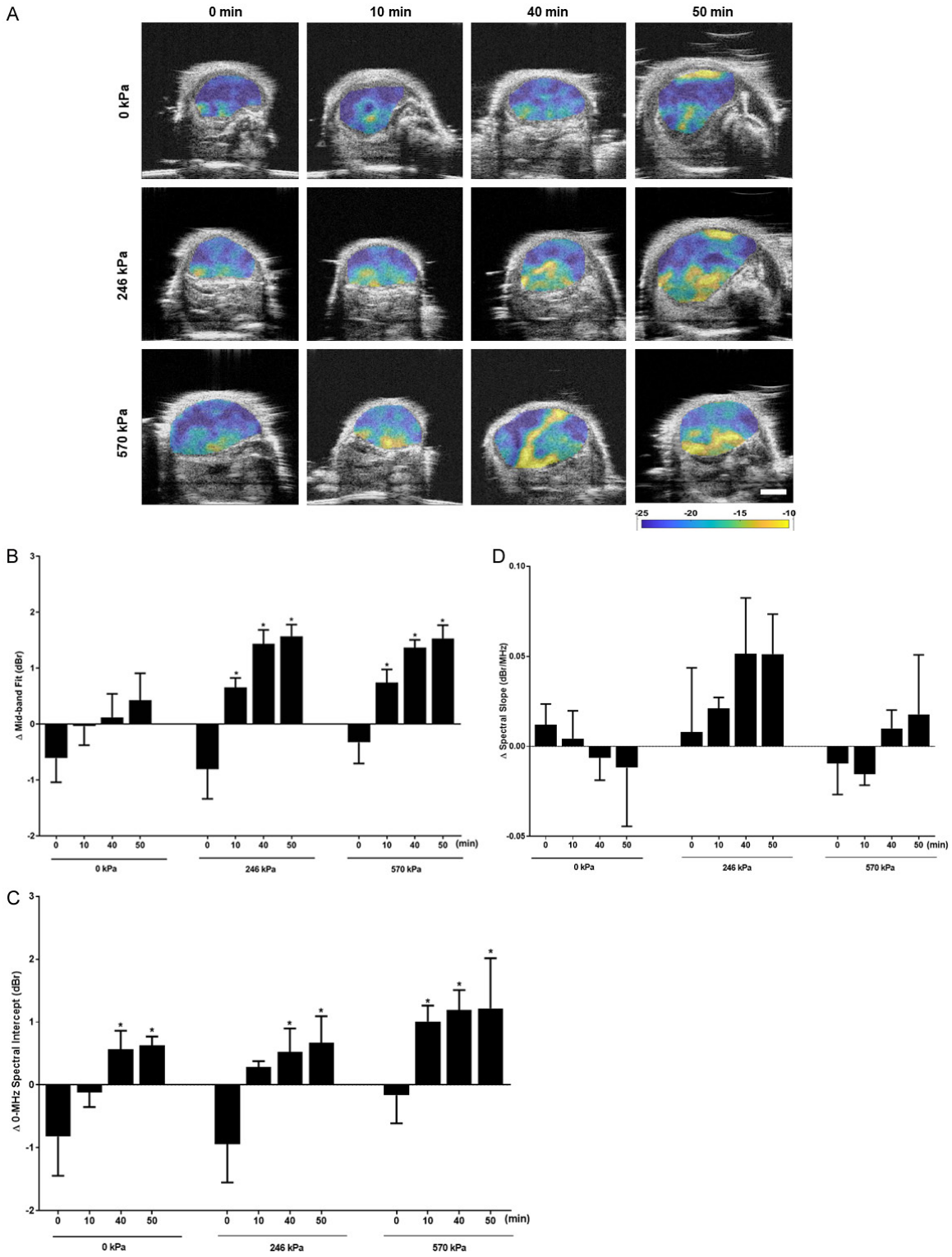

Figure 2. Representative parametric maps of MBF and plots displaying changes in quantitative ultrasound parameters at 24 hours followed USMB and HT. (A) MBF parametric images of PC3 tumors. Treatment conditions include HT only (0 kPa + 10 min, 0 kPa + 40 min, and 0 kPa + 50 min); and combined USMB and HT treatment (246 kPa + 0 min, 246 kPa + 10 min, 246 kPa + 40 min, and 246 kPa + 50 min); (570 kPa + 0 min, 570 kPa + 10 min, 570 kPa + 40 min, and 570 kPa + 50 min). Increases in the MBF intensity were observed most prominently with combined treatment of USMB and HT. The color scale represents a range of 20 dBr. Scale bar = 2 mm. Changes in average values of QUS spectral parameters (B) MBF (C) SI, and (D) SS obtained for PC3 xenografts after USMB and HT expo-

sure. Significant increases in the MBF and SI were observed with combined treatment of USMB and HT however no change in SS parameter was seen followed treatment. Error bars represent SEM (n = 3-5). Significance is indicated by * for (P<0.05) using a one-way ANOVA, Bonferroni selected comparisons. All conditions are compared to the control condition (0 kPa + 0 min).

was performed to determine statistically significant differences between untreated groups and other treatment groups. **Figure 2D** depicts averages changes in slope parameter. Results demonstrated that tumors treated with combined USMB and HT showed no significant changes in SS compared to control, USMB only treated group or HT only treated group (P>0.05).

Combined ultrasound-stimulated microbubbles and hyperthermia effects on tissue microstructure

H&E-stained tumor sections demonstrating disruptions in cell morphology were examined using high magnification microscopy as depicted in **Figure 3A**. Combinations of USMB and HT 246 kPa + 10 min; 246 kPa + 40 min; 246 kPa + 50 min, and 570 kPa + 10 min; 570 kPa + 40 min and 570 kPa + 50 min, displayed greater tumor cell disruption. H&E staining demonstrated an increase in apoptosis and necrosis after treatment. Apoptosis was confirmed in histology by associated morphological changes including nuclear coalescence and fragmentation, and the formation of apoptotic bodies. Additionally, cells were also found to undergo persistent cell shrinkage. On the other hand, cells undergoing necrosis exhibited distinct microscopic appearances like the dissolution of cellular organelles, cytoplasmic granulation, and cellular swelling. **Figure 3B** depicts high magnification representative images of TUNEL histology staining at 24 hours following USMB and HT treatment. Images indicate greater cell death (brown color) in combination-treated xenograft sections (246 kPa + 50 min; 570 kPa + 40 min and 570 kPa + 50 min) compared to the untreated group (0 kPa + 0 min). Quantification of TUNEL stained images in **Figure 3C** revealed a significant increase in cell death in tumors treated with the combination of USMB and HT. Combined treatment of 246 kPa + 50 min displayed greater cell death with 52.1 ± 4.8% death (P<0.05), whereas treating tumors with 570 kPa + 40 min and 570 kPa + 50 min showed tumor cell death of 27.5 ± 3.7% (P<0.05) and 30.1 ± 10.1% (P<0.05), respectively. Similarly, tumors that were treated with 0 kPa + 50 min also demonstrated a significant increase in cell death with 26.7 ± 8.5% (P<0.05) compared to 0 kPa + 0 min with 1.8 ± 0.4% cell death. However, 0 kPa + 10 min and 0 kPa + 40 min did not demonstrate any significant levels of cell death within tumor sections. A one-way ANOVA with Bonferroni selected comparison was performed to determine statistically significant differences between untreated groups and other treatment groups.

The correlations between cell death and ultrasound backscatter parameters in prostate cancer xenografts

Figure 4 shows scatter plots of cell death percentage as a function of (A) change in MBF, (B) change in SI, and (C) changes in MBF and in SI. An increase in backscattering due to cell death arising from a combination of USMB and HT treatments is reflected in the increase in both MBF and SI. The best-fit curves and surfaces are also shown. These indicate a correlation between cell death and changes in MBF and in SI. Quadratic regression fit of cell death with a change in MBF parameter resulted in a therapy predictive model with a fit function of % cell death = $4.6 \times \Delta MBF + 10.9 \times \Delta MBF^2 + 1.8$. The coefficient of determination to the fit was 0.81. Therapy predictive model developed using change in SI parameter resulted in a fit function of % cell death = $8.0 \times \Delta SI + 2.7 \times \Delta SI^2 + 9.5$. The coefficient of determination to the fit was 0.34. This indicates that change in MBF is more effective in predicting cell death compared to change in SI. This can be explained geometrically using linear fit, an increase in MBF implies an increase in SI, provided that the change in spectral slope is greater than or equal to 0, which might not always be satisfied. Using both changes in MBF and in SI, the best fit surface for therapy predictive model was % cell death = $16.2 \times \Delta MBF^2 + 3.8 \times \Delta SI^2 - 10.2 \times \Delta MBF \times \Delta SI + 1.2$. The coefficient of determination to the fit was 0.84. These R^2 values are comparable with a previous study that used a linear combination of acoustic scattering parameters and heterogeneity indices for developing therapy predictive models in a mouse model of breast cancer treated with chemotherapy [12].

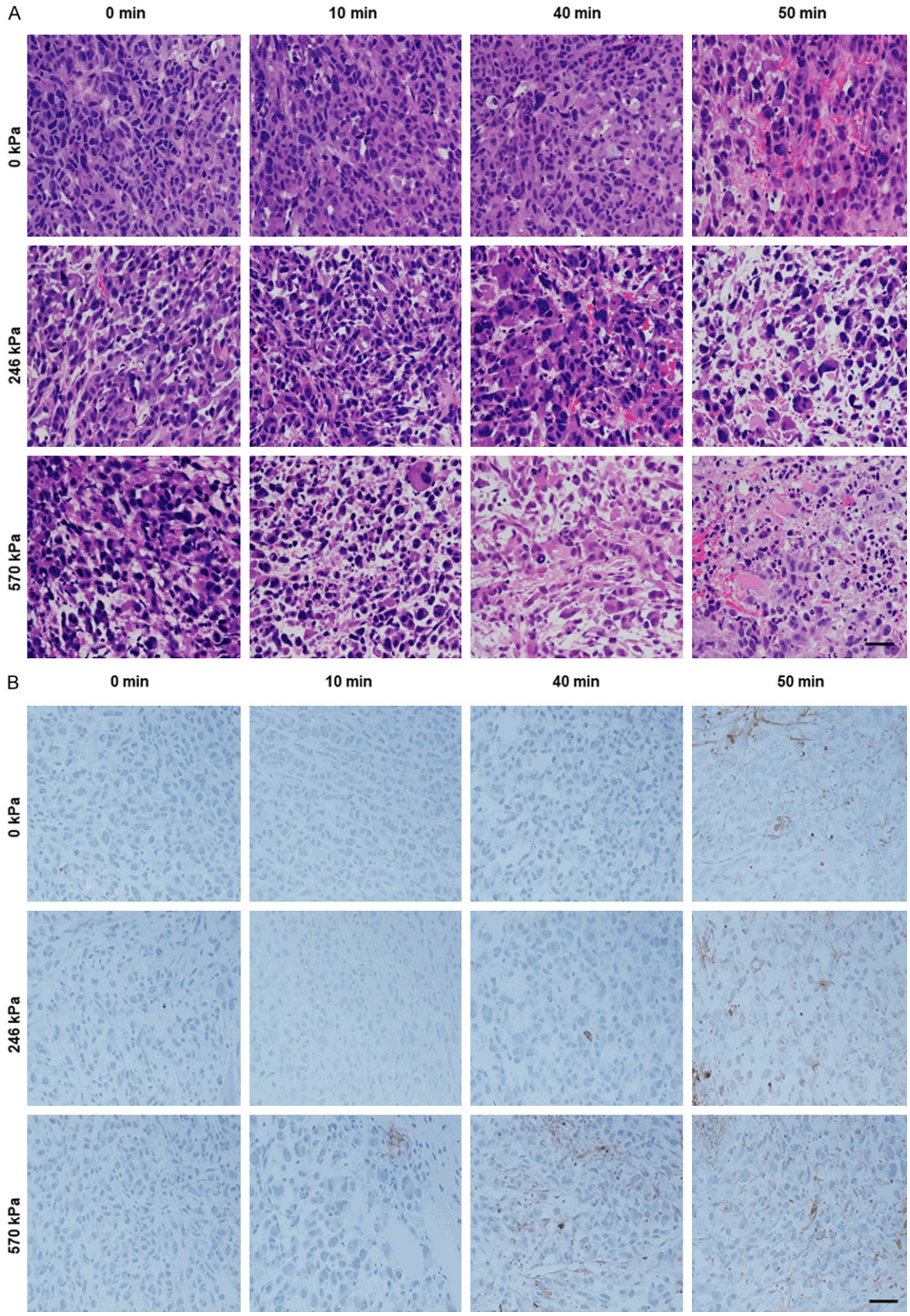
A
0 min
10 min
40 min
50 min
0 kPa
246 kPa
570 kPa
B
0 min
10 min
40 min
50 min
0 kPa
246 kPa
570 kPa

C

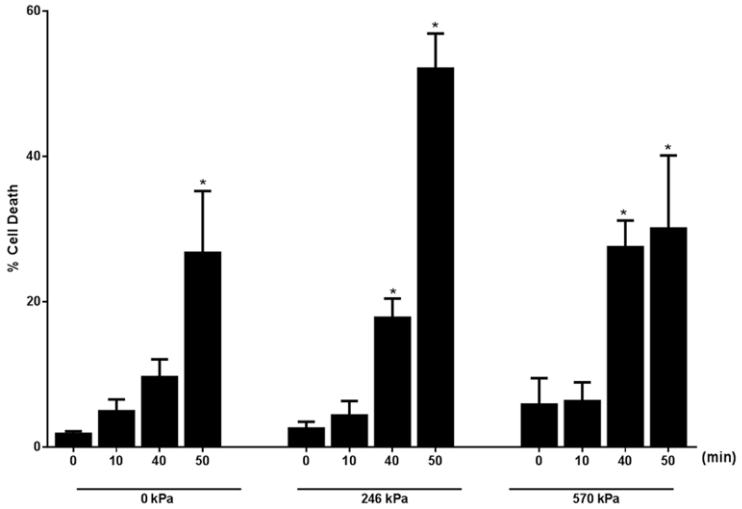

Figure 3. High magnification H&E, TUNEL staining, and quantification of tumor cell death of PC3 tumour xenografts followed USMB and HT. (A) H&E high magnification stained histological sections of PC3 tumor at 24 hours. Prominent cellular and tissue disruption were evident with the combined treatment 246 kPa + 10 min, 246 kPa + 40 min, 246 kPa + 50 min, and 570 kPa + 10 min, 570 kPa + 40 min, and 570 kPa + 50 min. Images were obtained at 20 × magnification. The scale bar represents 50 μm. (B) TUNEL stained histological sections of PC3 treated tumor at 24 hours. Top panels represent 0 kPa with HT duration 0, 10, 40, and 50 min, middle panels represent 246 kPa with similar HT durations, and bottom panels represent 570 kPa with similar HT durations. The scale bar represents 50 μm. (C) Quantification of tumor cell death per treatment group determined from TUNEL stained histology sections from 24 hours. A maximum increase in cell death was observed in combined treatment (246 kPa + 50 min). An increase in cell death is also observed with 0 kPa + 50 min, 570 kPa + 40 min, and 570 kPa + 50 min. Error bars represent SEM (n = 3-5). Significance is indicated by * for (P<0.05) using a one-way ANOVA, Bonferroni selected comparisons. All conditions are compared to the control condition (0 kPa + 0 min). Cell death graph adapted with permission from [32].

Statistical analysis

Statistical analysis was conducted using Graph Pad Prism software (Graph Pad Software, La Jolla, CA, USA) using analysis of variance (ANOVA) followed by Bonferroni's selected comparisons test. *P*-values (P<0.05) were considered statistically significant and are indicated by asterisk*.

Discussion

QUS backscatter parameters including MBF, SI, and SS have been previously used for the characterization of multiple xenograft tissues [10, 24-26]. The motivation of the current work is based on previous findings suggesting that QUS can be used to study the effects of cell death on ultrasound spectral parameters [11, 25, 27]. This study aimed to expand the use of QUS in determining changes in ultrasound backscatter parameters with cell death followed HT therapy. In the present study, QUS was investigated for monitoring a combination of treatments using USMB and HT treatment in prostate cancer xenografts at 24 hours after treatment. In particular, ultrasound-based spectral parameters, such as MBF, SI, and SS parameters were determined. Separately, changes in cellular structures within the tissue samples were assessed.

The data here demonstrated significant changes in ultrasound backscatter parameters (MBF and SI) with combined treatment. Significant increases in MBF with combined treatments 246 kPa + 10 min (P<0.05), 246 kPa + 40 min (P<0.05), 246 kPa + 50 min (P<0.05) and 570 kPa + 10 min (P<0.05), 570 kPa + 40 min (P<0.05), and 570 kPa + 50 min (P<0.05) were observed compared to the control (0 kPa + 0 min) (**Figure 2B**). Similarly, combined treatment induced a greater increase in SI compared to the untreated group (**Figure 2C**). The results indicated a significant enhancement in cell death with changes in cell and tissue structures followed the combined treatment of 246 kPa + 50 min (P<0.05), 570 kPa + 40 min

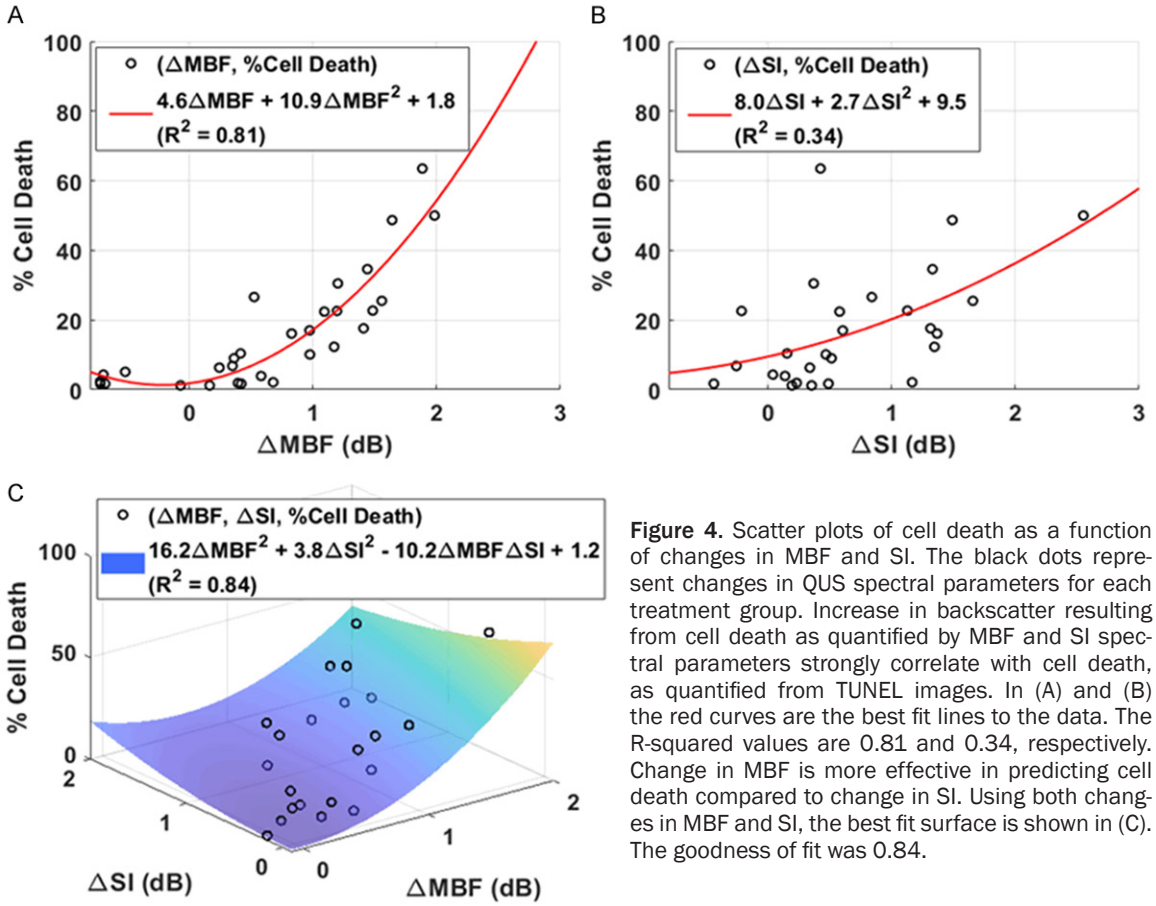

Figure 4. Scatter plots of cell death as a function of changes in MBF and SI. The black dots represent changes in QUS spectral parameters for each treatment group. Increase in backscatter resulting from cell death as quantified by MBF and SI spectral parameters strongly correlate with cell death, as quantified from TUNEL images. In (A) and (B) the red curves are the best fit lines to the data. The R-squared values are 0.81 and 0.34, respectively. Change in MBF is more effective in predicting cell death compared to change in SI. Using both changes in MBF and SI, the best fit surface is shown in (C). The goodness of fit was 0.84.

(P<0.05), and 570 kPa + 50 min (P<0.05) (**Figure 3A-C**). These were confirmed using assessments of H&E and TUNEL immunohistochemistry. This was consistent with previous work which demonstrated that with various treatment modalities like radiation therapy or chemotherapy, ultrasound backscatter parameters change as a result of nuclear material aggregation associated with tumor cell death [11, 25, 28].

Several rationales have been reported in connection to changes in ultrasound backscatter with cell death. These mainly correspond to changes in tumor morphological characteristics during the cell death process. The process of programmed cell death, or apoptosis, starts with blebbing of cell membranes leading to degraded organelle compartmentalization, followed by DNA fragmentation into multiple vesicles called apoptotic bodies [29]. These changes a single large scattering structure of the cell to more densely packed small structures causing an increase in backscatter. Such changes in backscatter phenomena have been reported using both low and high (>10 MHz) frequency ultrasound [24]. An early study demonstrated that cells undergoing apoptosis exhibited more than twofold increase in ultrasound backscatter compared to viable cells at 24 hours [4]. Work by Sadeghi-Naini *et al.* indicated prostate xenografts upon exposure to radiation and USMB therapy exhibited unique morphological features including cells appearing swollen, undergoing the process of nuclear pyknosis and mitotic catastrophe. Associated ultrasound results demonstrated a significant increase in MBF (5.9 ± 0.9 dBr) and SI (4.8 ± 1.2 dBr) compared to untreated group (0.1 ± 0.2 dBr) and (-0.3 ± 0.6 dBr), respectively [24]. Prior to this, Lee *et al.* observed a similar correlation between increased cell death and ultrasound backscatter parameters revealing a 63 ± 5% increase in cell death with corresponding increases in the MBF (5.2 ± 1.4 dBr) and SI (6.3 ± 1.9 dBr) following USMB and radiation treatments of tumor xenografts [30]. Additionally, an increase in MBF and SI corresponding to an

increase in cell fragmentation was also reported in a different study using the same treatment type [26]. A similar study conducted by Tran *et al.* in bladder tumor xenografts demonstrated that a combination of radiation and USMB induced an increase in MBF (6.41 ± 1.40 dBr) and an increase in SI (7.01 ± 1.20 dBr). The study indicated greater areas of cell death within the treated tumor which contributed to the increase in MBF and SI [25].

It is worth noting that our results demonstrated no changes in the slope parameter with the treatment of USMB and HT (**Figure 2D**). A study by Kim *et al.* observed an inverse relationship between MBF/SI and SS. Their result showed that with increasing microbubble concentration and radiation doses the SS decreased [26]. The SS is an indicator of scatterer size and an increase in SS has been shown to correspond to a decrease in scatterer size [11]. Therefore, a reduction in scatterer size is expected as the result of an increase in treatment parameters. However, in our study, no changes in scatterer size can be rationalized with the range of ultrasound frequencies used. As suggested earlier, the most accurate measurements of scatterer sizes are when the scatterer size~wavelength [31]. At 25 MHz center frequency, the estimated scatterer size is 3-4 times the size of a tumor cell, therefore referring to aggregates of tumor cells undergoing apoptosis and necrosis. Therefore, size estimation alone of this patch of tumor cells does not provide inference on how the scatterer's organization is altered, which results in an increase in backscattering as quantified from MBF and SI parameters.

Whereas most studies have focused on one or two forms of cell death, mainly apoptosis, a study by Pasternak *et al.* characterized several modes of cell death including apoptosis-induced upon cisplatinum treatment, ischemia-induced oncosis, colchicine-induced mitotic arrest, and heat-induced cell death using high-frequency ultrasound. The study demonstrated an increase in MBF value from -49.8 ± 0.6 dBr to -42.7 ± 1.2 dBr within 24 hours following cisplatinum treatment to induce apoptosis. The colchicine-induced mitotic arrest caused similar increases in ultrasound backscatter. This trend remained elevated with further time duration including 48 and 72 hours. In contrast, samples undergoing oncosis demonstrated a decrease in MBF following 72 hours. Similarly, samples undergoing heat-induced cell death exhibited no increase in MBF. In addition, the SI data was found to generally mirror the results obtained from MBF [28].

It should be noted that while most studies have demonstrated that the aggregation of nuclear material during the cell death process results in the enhancement of backscatter intensity, a reverse phenomenon with the digestion of nuclear material resulting in decrease backscatter signal is also reported during the late apoptosis stage. Banihashemi and colleagues observed a significant increase in MBF as early as 12-24 hours whereas by 48 hours the MBF value significantly dropped following photodynamic therapy in a melanoma xenograft model [11].

In the work here, histopathology indicated significantly higher fragments of condensed DNA, an increase in the number of apoptotic bodies as well as shrinkage in cell size which was confirmed by H&E staining using high magnification microscopy (**Figure 3A**). Furthermore, in the work here there were tumor regions with erythrocytes with combined treatment which might be due to extensive vascular disruption, as also observed in other work [25].

The acute and longitudinal treatment effects in prostate cancer xenograft of the treatments here are reported elsewhere [32]. The work demonstrated a significant decrease in vascular density and significantly fewer proliferating cells with greater inhibition in tumor growth followed combined USMB and HT treatments. This was linked to greater condensed and fragmented nuclear materials and ruptured plasma membranes, classically considered as hallmarks of apoptotic and necrotic cells, respectively. The present work is the first to investigate changes in backscatter parameters and associated tissue structural changes resulting from a novel combination of USMB and HT treatments. The outcome presented in this study forms a basis for using QUS methodology non-invasively to track microbubble-based HT-enhancement.

Acknowledgements

G.J. Czarnota is supported by a James and Mary Davie Chair in Breast Cancer Imaging and Therapy. This research was supported by

grants from the Canadian Cancer Society Research Institute (CCSRI).

Disclosure of conflict of interest

None.

Address correspondence to: Dr. Gregory J Czarnota, Department of Radiation Oncology, Sunnybrook Health Sciences Centre, 2075 Bayview Avenue, Toronto, Ontario M4N 3M5, Canada. Tel: 416-480-6128; Fax: 416-480-6002; E-mail: gregoryczarnota.submissions@gmail.com; Gregory.Czarnota@sunnybrook.ca

References

[1] Majno G and Joris I. Apoptosis, oncosis, and necrosis: an overview of cell death. Am J Pathol 1995; 146: 3-15.

[2] Castedo M, Perfettini JL, Roumier T, Andreau K, Medema R and Kroemer G. Cell death by mitotic catastrophe: a molecular definition. Oncogene 2004; 23: 2825-2837.

[3] Kim YS, Rhim H, Lim HK, Choi D, Lee MW and Park MJ. Coagulation necrosis induced by radiofrequency ablation in the liver: histopathologic and radiologic review of usual to extremely rare changes. Radiographics 2011; 31: 377-390.

[4] Czarnota GJ, Kolios MC, Vaziri H, Benchimol S, Ottensmeyer FP, Sherar MD and Hunt JW. Ultrasonic biomicroscopy of viable, dead and apoptotic cells. Ultrasound Med Biol 1997; 23: 961-965.

[5] Czarnota GJ, Kolios MC, Abraham J, Portnoy M, Ottensmeyer FP, Hunt JW and Sherar MD. Ultrasound imaging of apoptosis: high-resolution non-invasive monitoring of programmed cell death in vitro, in situ and in vivo. Br J Cancer 1999; 81: 520-527.

[6] Gonzalez VM, Fuertes MA, Alonso C and Perez JM. Is cisplatin-induced cell death always produced by apoptosis? Mol Pharmacol 2001; 59: 657-663.

[7] Zhu J, Okumura H, Ohtake S, Nakamura S and Nakao S. The molecular mechanism of arsenic trioxide-induced apoptosis and oncosis in leukemia/lymphoma cell lines. Acta Haematol 2003; 110: 1-10.

[8] Weerasinghe P and Buja LM. Oncosis: an important non-apoptotic mode of cell death. Exp Mol Pathol 2012; 93: 302-308.

[9] Kolios MC, Czarnota GJ, Lee M, Hunt JW and Sherar MD. Ultrasonic spectral parameter characterization of apoptosis. Ultrasound Med Biol 2002; 28: 589-597.

[10] Vlad RM, Brand S, Giles A, Kolios MC and Czarnota GJ. Quantitative ultrasound characterization of responses to radiotherapy in cancer mouse models. Clin Cancer Res 2009; 15: 2067-2075.

[11] Banihashemi B, Vlad R, Debeljevic B, Giles A, Kolios MC and Czarnota GJ. Ultrasound imaging of apoptosis in tumor response: novel preclinical monitoring of photodynamic therapy effects. Cancer Res 2008; 68: 8590-8596.

[12] Tadayyon H, Sannachi L, Sadeghi-Naini A, Al-Mahrouki A, Tran WT, Kolios MC and Czarnota GJ. Quantification of ultrasonic scattering properties of in vivo tumor cell death in mouse models of breast cancer. Transl Oncol 2015; 8: 463-473.

[13] Kiessling F, Bzyl J, Fokong S, Siepmann M, Schmitz G and Palmowski M. Targeted ultrasound imaging of cancer: an emerging technology on its way to clinics. Curr Pharm Des 2012; 18: 2184-2199.

[14] Gwag BJ, Koh JY, Chen MM, Dugan LL, Behrens MM, Lobner D and Choi DW. BDNF or IGF-I potentiates free radical-mediated injury in cortical cell cultures. Neuroreport 1995; 7: 93-96.

[15] Sanders EJ and Wride MA. Programmed cell death in development. Int Rev Cytol 1995; 163: 105-173.

[16] Sohn S, Kim EY and Gwag BJ. Glutamate neurotoxicity in mouse cortical neurons: atypical necrosis with DNA ladders and chromatin condensation. Neurosci Lett 1998; 240: 147-150.

[17] Sadeghi-Naini A, Papanicolau N, Falou O, Zubovits J, Dent R, Verma S, Trudeau M, Boileau JF, Spayne J, Iradji S, Sofroni E, Lee J, Lemon-Wong S, Yaffe M, Kolios MC and Czarnota GJ. Quantitative ultrasound evaluation of tumor cell death response in locally advanced breast cancer patients receiving chemotherapy. Clin Cancer Res 2013; 19: 2163-2174.

[18] Sannachi L, Tadayyon H, Sadeghi-Naini A, Tran W, Gandhi S, Wright F, Oelze M and Czarnota G. Non-invasive evaluation of breast cancer response to chemotherapy using quantitative ultrasonic backscatter parameters. Med Image Anal 2015; 20: 224-236.

[19] Tadayyon H, Sadeghi-Naini A, Wirtzfeld L, Wright FC and Czarnota G. Quantitative ultrasound characterization of locally advanced breast cancer by estimation of its scatterer properties. Med Phys 2014; 41: 012903.

[20] Sadeghi-Naini A, Suraweera H, Tran WT, Hadizad F, Bruni G, Rastegar RF, Curpen B and Czarnota GJ. Breast-lesion characterization using textural features of quantitative ultrasound parametric maps. Sci Rep 2017; 7: 13638.

[21] Liao YY, Tsui PH, Li CH, Chang KJ, Kuo WH, Chang CC and Yeh CK. Classification of scattering media within benign and malignant breast tumors based on ultrasound texture-feature-based and nakagami-parameter images. Med Phys 2011; 38: 2198-2207.

[22] Alvarenga AV, Pereira WC, Infantosi AF and Azevedo CM. Complexity curve and grey level co-occurrence matrix in the texture evaluation of breast tumor on ultrasound images. Med Phys 2007; 34: 379-387.
[23] Garra BS, Krasner BH, Horii SC, Ascher S, Mun SK and Zeman RK. Improving the distinction between benign and malignant breast lesions: the value of sonographic texture analysis. Ultrason Imaging 1993; 15: 267-285.
[24] Sadeghi-Naini A, Papanicolau N, Falou O, Tadayyon H, Lee J, Zubovits J, Sadeghian A, Karshafian R, Al-Mahrouki A, Giles A, Kolios MC and Czarnota GJ. Low-frequency quantitative ultrasound imaging of cell death in vivo. Med Phys 2013; 40: 082901.
[25] Tran WT, Sannachi L, Papanicolau N, Tadayyon H, Al Mahrouki A, El Kaffas A, Gorjizadeh A, Lee J and Czarnota GJ. Quantitative ultrasound imaging of therapy response in bladder cancer in vivo. Oncoscience 2016; 3: 122-133.
[26] Kim HC, Al-Mahrouki A, Gorjizadeh A, Sadeghi-Naini A, Karshafian R and Czarnota GJ. Quantitative ultrasound characterization of tumor cell death: ultrasound-stimulated microbubbles for radiation enhancement. PLoS One 2014; 9: e102343.
[27] El Kaffas A, Gangeh MJ, Farhat G, Tran WT, Hashim A, Giles A and Czarnota GJ. Tumour vascular shutdown and cell death following ultrasound-microbubble enhanced radiation therapy. Theranostics 2018; 8: 314-327.
[28] Pasternak MM, Sadeghi-Naini A, Ranieri SM, Giles A, Oelze ML, Kolios MC and Czarnota GJ. High-frequency ultrasound detection of cell death: spectral differentiation of different forms of cell death in vitro. Oncoscience 2016; 3: 275-287.
[29] Cotter TG. Apoptosis and cancer: the genesis of a research field. Nat Rev Cancer 2009; 9: 501-507.
[30] Lee J, Karshafian R, Papanicolau N, Giles A, Kolios MC and Czarnota GJ. Quantitative ultrasound for the monitoring of novel microbubble and ultrasound radiosensitization. Ultrasound Med Biol 2012; 38: 1212-1221.
[31] Insana MF and Hall TJ. Parametric ultrasound imaging from backscatter coefficient measurements: image formation and interpretation. Ultrason Imaging 1990; 12: 245-267.
[32] Sharma D, Giles A, Hashim A, Yip J, Ji Y, Do NNA, Sebastiani J, Tran WT, Farhat G, Oelze M and Czarnota GJ. Ultrasound microbubble potentiated enhancement of hyperthermia-effect in tumours. PLoS One 2019; 14: e0226475.